$D^{*\pm}$ Production in e^-p and e^+p Deep Inelastic Scattering at HERA*

S. D. Robins

on behalf of the ZEUS collaboration

Inclusive production of $D^{*\pm}(2010)$ mesons in deep inelastic scattering has been measured using e^+p and e^-p data obtained with the ZEUS detector at HERA using integrated luminosities of 16.7 and 65.2pb^{-1}, respectively. The decay channel $D^{*+} \to D^0\pi^+$ with $D^0 \to K^-\pi^+$ and corresponding antiparticle decays were used to identify $D^{*\pm}$ mesons. The $D^{*\pm}$ cross sections in e^-p and e^+p interactions agree with NLO QCD predictions, although the $D^{*\pm}$ cross section in e^-p is slightly higher than that in e^+p.

1. Introduction

Charm production in deep inelastic scattering (DIS) at HERA has been shown in previous studies to be consistent with purely dynamic Boson-Gluon Fusion (BGF) production [1–3]. This agreement has now been tested with a larger data sample than the previous ZEUS measurements, and e^-p as well as e^+p cross sections have been calculated. The charmed mesons were identified using the decay $D^{*+} \to D^0\pi^+$ with $D^0 \to K^-\pi^+$ and corresponding antiparticle processes, where π_s refers to a low momentum pion accompanying the D^0. The differential cross sections are measured as functions of Q^2 and Bjorken x, defined as $Q^2 = -q^2 = (k - k')^2$ and $x = Q^2/(2P \cdot q)$, where k and k' are the four-momenta of the initial and final state lepton, and P is the four-momentum of the proton.

2. Kinematic reconstruction and event selection

The ZEUS detector is described in detail elsewhere [4, 5]. The x and Q^2 variables were reconstructed by the Σ-method, which uses both the scattered lepton and the hadronic system measurements [6]. Standard cuts were imposed to select neutral current DIS events [7]. The $D^{*\pm}$ mesons

* Presented at DIS02

were selected in the range $1.80 < M(D^0) < 1.92$ GeV, $0.143 < \Delta M < 0.148$ GeV, $1.5 < p_T(D^*) < 15$ GeV, and $|\eta(D^*)| < 1.5$. The number of $D^{*\pm}$ events determined from a 5 parameter fit

$$F(\Delta M) = [P1/\sqrt{2\pi} \cdot P3] \cdot exp[0.5 \cdot (\Delta M - P2)^2/P3] + P4 \cdot (\Delta M - m_\pi)^{P5}$$

where $P1$ - $P5$ are free parameters is 1229 ± 48 in the $e^- p$ data, and 4240 ± 90 in the $e^+ p$ data. The number of $D^{*\pm}$ mesons extracted from empirical wrong charge background subtraction within the signal region $143 < \Delta M < 148$ MeV, is 1219 ± 58 and 4239 ± 113 in the $e^- p$ and $e^+ p$ data respectively. The ΔM distributions are shown in Figure 1, for $e^- p$ and $e^+ p$ data separately.

3. Study of systematic effects

The systematic uncertainties on the measured $D^{*\pm}$ cross sections were determined by changing the selection cuts or analysis procedure. These uncertainties are divided into three groups.

Event reconstruction and selection:

- The cuts on y_e. $y_J B$, δ, and the vertex position were varied [7].
- The cut on the position of the scattered lepton in the RCAL was raised.
- The minimum energy of the scattered lepton was raised.
- The Electron method or Double Angle method [8] was used to reconstruct the kinematics.

$D^{*\pm}$ reconstruction:

- A higher track quality was required (restriction on the polar angle of the track).
- The transverse momentum requirement of the K and π candidates was varied.
- The signal region for $M(D^0)$ and ΔM were varied.

Monte Carlo:

- The acceptance was calculated using HERWIG [9] instead of RAPGAP [10].

The overall systematic uncertainty was determined by adding the above uncertainties in quadrature. The normalisation uncertainties due to the luminosity measurement error, and those due to the $D^{*\pm}$ and D^0 branching ratios were not included.

4. Results

In the kinematic region $1 < Q^2 < 1000$ GeV^2, $0.02 < y < 0.08$ and the selected $D^{*\pm}$ region, the cross sections calculated are

$$\sigma(e^- p \to e^- D^{*\pm} X) = 10.20 \pm 0.48(stat.)^{0.36}_{0.54}(syst.) \text{ nb},$$

$$\sigma(e^+ p \to e^+ D^{*\pm} X) = 8.94 \pm 0.24(stat.)^{0.27}_{0.51}(syst.) \text{ nb}.$$

The e^+p cross section is consistent with that previously published [1], allowing for the increase in proton beam energy [7], while the e^-p cross section is slightly higher. Figure 2 shows the differential cross sections as a function of Q^2 and x compared to the NLO calculation implemented in the HVQDIS program [11, 12]. This program is based on the BGF mechanism, and uses the Peterson fragmentation function [13], with $\epsilon = 0.035$, to hadronise the charm quark to a $D^{*\pm}$. The mass and renormalisation scales were set to $\sqrt{4m_c^2 + Q^2}$. The hadronisation fraction $f(c \to D^{*+})$ was set to 0.235 [14]. The boundaries of the shaded band indicate two extreme values of HVQDIS predictions, from changing the charm mass between $m_c = 1.3$ to 1.6 GeV, and using different sets of structure functions, GRV98HO [15], CTEQ5F3 [16] and a ZEUS NLO fit [17]. The NLO calculations based on BGF give a good description of the measured $D^{*\pm}$ cross section over the full range of Q^2 and x. For $Q^2 > 20$ GeV^2, the $D^{*\pm}$ cross sections in e^-p and e^+p differ slightly, while conventional charm production mechanisms contain no charge dependence on the lepton in these interactions. More e^-p data is essential to investigate whether this is a statistical fluctuation.

References

[1] ZEUS Coll., J. Breitweg *et al.*, Eur. Phys. J. **C 12**, 35 (2000).

[2] H1 Coll., C. Adloff *et al.*, Z. Phys. **C 72**, 593 (1996).

[3] ZEUS Coll., J. Breitweg *et al.*, Phys. Lett. **B 407**, 402 (1997).

[4] ZEUS Coll., M. Derrick *et al.*, Phys. Lett. **B 293**, 465 (1992).

[5] ZEUS Coll., M. Derrick *et al.*, Z. Phys. **C 63**, 391 (1994).

[6] U. Bassler and G. Bernardi, Nucl. Inst. Meth. **A 361**, 197 (1995).

[7] ZEUS Coll., $D^{*\pm}$ *Production in Deep Inelastic Scattering*, 2001.

[8] S. Bentvelsen, J. Engelen and P. Kooijman, in *Proc. Workshop on Physics at HERA*, eds. W. Buchmüller and G. Ingelman, Vol. 1, p. 23. Hamburg, Germany, DESY, 1992.

[9] G. Marchesini *et al.*, Comp. Phys. Comm. **67**, 465 (1992).

[10] H. Jung, Comp. Phys. Comm. **86**, 147 (1995).

[11] B.W. Harris, J. Smith, PL **B 353**, 535 (1995).
[12] B.W. Harris, J. Smith, PR **D 57**, 2806 (1995).
[13] C. Peterson *et al.*, Phys. Rev. **D 27**, 105 (1983).
[14] L. Gladilin, Preprint hep-ex/9912064, 1999.
[15] M. Glück, E. Reya and A. Vogt, Eur. Phys. J. **C 5**, 461 (1998).
[16] CTEQ Coll., H.L. Lai *et al.*, Eur. Phys. J. **C 12**, 375 (2000).
[17] ZEUS Coll., J. Breitweg *et al.*, Eur. Phys. J. **C 7**, 609 (1999).

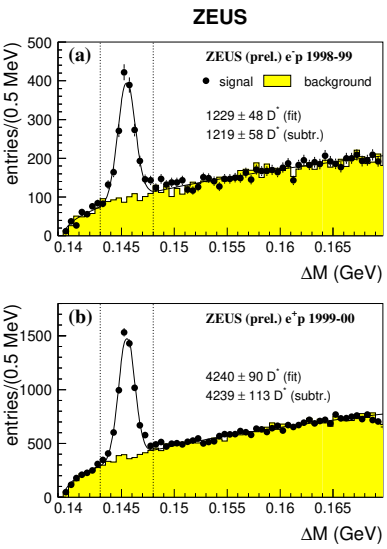

Fig. 1. *Data (solid dots) for* $\Delta M = (M_{K\pi\pi_s} - M_{K\pi})$ *for* e^-p *data above and* e^+p *data below. The background from wrong charge combinations in shown as the filled histogram. The solid line shows the result of the fit described in the text; the dashed vertical line indicates the signal region.*

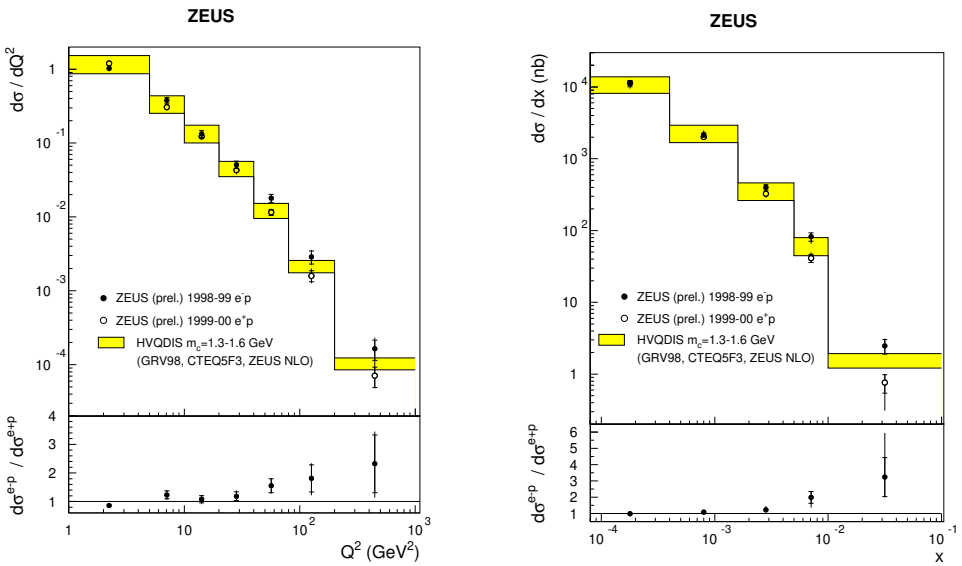

Fig. 2. *Differential* $D^{*\pm}$ *cross sections for* e^-p *and* e^+p *data as a function of* Q^2 *on the left and* x *on the right, compared to the NLO QCD calculation of HVQDIS. The inner error bars show the statistical uncertainties, while the outer ones are the statistical and systematic errors added in quadrature. The boundaries of the shaded band for the HVQDIS prediction correspond to the full uncertainty due to the charm mass variation and choice of structure function as described in the text. The lower portion of each plot shows the ratio of the* e^-p *to* e^+p *cross sections.*